A Genetic Algorithm for Joint Power and Bandwidth Allocation in Multibeam Satellite Systems

Aleix Paris, Inigo del Portillo, Bruce Cameron, Edward Crawley
Massachusetts Institute of Technology
77 Massachusetts Avenue 33-409
Cambridge, MA 02139
{aleix, portillo, bcameron, crawley}@mit.edu

***Abstract*—Communications satellites are becoming more flexible and capable in order to make better use of on-board resources and the available spectrum, and to satisfy the varying demands within the satellite broadband market. New generations of communications satellites will provide hundreds of Gbps of throughput by using advanced digital payloads, which will allow for beam-steering and beam-shaping, in addition to individual allocation of power and bandwidth for each beam. Therefore, dynamic resource management (DRM) techniques for communications satellites will be crucial for operators to fully exploit the capabilities of their satellites.**

This paper presents a new method for joint power and bandwidth allocation in multibeam satellite systems. To that end, we first develop a multibeam satellite model that accounts for propagation effects, interference among beams, and atmospheric attenuation. Next, we formulate the joint power and bandwidth allocation optimization problem and propose a novel algorithm to solve it. The basis of this algorithm is a genetic algorithm that is combined with repair functions to guarantee the validity of the solutions and speed up convergence.

Finally, the usefulness of the algorithm is analyzed through two case studies: a notional case featuring a 37-beam satellite and a realistic case based on Viasat-1. The results obtained show that our joint power and bandwidth allocation algorithm can reduce the unmet system capacity (USC) by up to 40% (compared to just power allocation approaches). Furthermore, our experiments identify the variation of the demand among beams as a parameter that has a large impact on potential improvement: the higher the variation in demand among beams, the more beneficial it is to allow a greater flexibility in the range of bandwidth allocations allowed.

TABLE OF CONTENTS

978-1-5386-6854-2/19/$31.00

1. INTRODUCTION

Motivation

The communications satellites market has experienced disruptive technological advancements in the last 10 years driven by the need to satisfy the increasing demand for connectivity services in remote locations not served by ground infrastructure, and the expansion of the mobility sector (airplanes and ships) [1].

Spot beams have been one of the most significant advancements leading to the increase in capacity in modern satellites. In a spot beam the signal power is focused on a specific area of the Earth's surface, being the beam's footprint on the order of several hundreds of kilometers. Current-generation high-throughput satellites (HTS) – such as ViaSat-2 and EchoStar 24 – provide 300 - 600 Gbps of capacity and have hundreds of beams. Future generations such as ViaSat-3 or SES's mPower MEO constellation will have thousands of beams and capacities in the Tbps range. Finally, phased-array antenna technology is being introduced into next-generation satellites, enhancing the capabilities of spot beams by allowing for reconfigurable numbers of beams, boresight pointing, and beamforming.

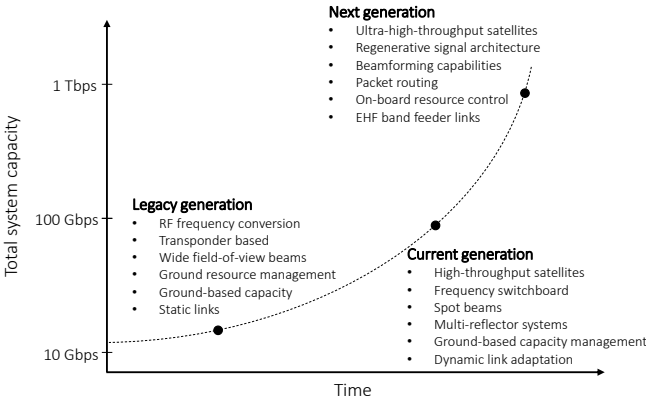

Figure 1: **Technological advancements in successive generations of communications satellites. Adapted from [4].**

To further expand the capabilities of their satellites and serve the rising demand, operators are transitioning from rigid bent-pipe architectures towards flexible and reconfigurable satellite architectures [2], as shown in Fig. 1; in newer designs analog payloads are replaced with digital payloads, which allow for dynamic on-demand resource allocation [3]. In particular, whereas older generations of satellites had a bent-pipe architecture (the uplink signal was relayed back to Earth

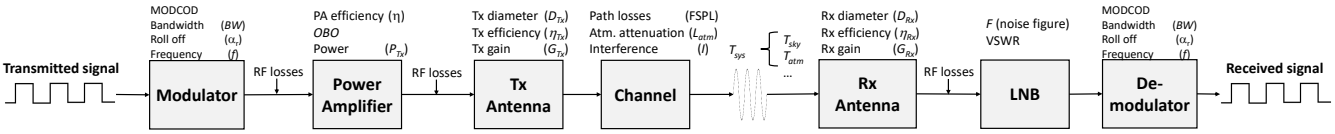

Figure 2: **Link model block diagram**

through a particular beam after being amplified and shifted in frequency), new satellites provide advanced adaptability such as dynamic power and bandwidth allocations, beam shaping and beam steering, signal demodulation and remodulation, routing capabilities, etc.

However, with greater flexibility comes increased complexity. The larger number of beams and multiple configurable variables for each of them (power, bandwidth, boresight pointing, etc.) requires the use of advanced techniques for dynamic resource management (DRM), which has become a popular topic of research both in industry and academia due to the increasing number of companies planning to launch satellites with flexible architectures. Among others, SES (mPower, SES-17), Telesat, Intelsat, and SpaceX (Starlink) have scheduled launches of such systems within the next 5 years.

Literature Review

The optimization of resource allocation in communications satellites has been addressed from different perspectives. A number of studies focused on *temporal beam hopping techniques* [5], [6], [7], where only a fraction of the beams are active at a given time. In particular, the authors in [5] proposed a genetic algorithm to optimize the active beams' time plan, whereas [6] analyzed the advantages of applying beam hopping to conventional satellite systems.

Another approach is *cognitive satellite communications* [8], which is based on actively monitoring the spectrum allocated to other systems and exploiting it when not being used. Authors in [9] and [10] proposed beamforming and bandwidth allocation in a spectral coexistence scenario of satellites and ground users, while in [11] the authors proposed a distributed power control algorithm based on the signal to interference plus noise ratio for cognitive satellite networks.

Finally, with regard to algorithms for *power and/or bandwidth allocation*, Aravanis et al. [12] developed a hybrid genetic algorithm and simulated annealing method to allocate power to each beam so that the unmet system capacity (USC) and the total power used were minimized. In [13], besides power, carrier allocation was also considered to minimize the co-channel interference using an analytical approach based on the axiomatic interference model to balance the signal-to-interference-plus-noise ratio (SINR). The authors in [14] used the method of Lagrange multipliers to allocate power and bandwidth considering the delay bounds of real-time packages, though only a simple system comprising one link and a few users was studied. This type of delay-sensitive traffic was also considered in [15], where the authors presented an algorithm based on the non-dominated sorting genetic algorithm II (NSGA-II) to jointly allocate frequency-time resource blocks and power. Using their approach, they obtained the Pareto front of the throughput vs. the call completion ratio. Nevertheless, interference between beams was not modeled and instead the authors limited frequency reuse. A similar Lagrange multipliers-based approach was taken in reference [16], where the return link was optimized after satisfying the forward link requirements. Finally, based on the duality theory, the authors in [17] developed an iterative power and bandwidth allocation algorithm that penalized delays, but it ignored interference between beams.

This literature review reveals that there is a gap in existing research, in that multibeam-satellite algorithms that allocate both power and bandwidth (while considering important factors such as the interference between beams) have not yet been addressed.

Research Goals

This paper has a twofold objective:

- First, to develop a new methodology for joint power and bandwidth allocation in multibeam satellite systems by extending the approach described in [12], which only considered power allocation.
- To investigate the performance improvement obtained by dynamically allocating bandwidth, as compared to previous studies where only power was allocated.

Paper Organization

This paper is organized as follows: Section 2 presents the system models, which include the link budget, interference, and atmospheric attenuation models; Section 3 introduces the mathematical formulation of the problem; Section 4 describes the new proposed algorithm; Section 5 introduces two case studies that will be used to evaluate the new algorithm; Section 6 presents the results for these case studies, whose bandwidth and power allocations are optimized under different demand scenarios; and Section 7 concludes the paper by highlighting the main results and contributions, and proposing areas of future research.

2. SYSTEM MODELS

The objective of this section is to describe the models as well as the assumptions made within this paper.

Link Budget Model

Figure 2 shows an overview of the link-model, as well as the parameters considered by each of the blocks. These parameters are the inputs for the link-budget equation, which is used to compute the achievable data rate for each of the beams. As can be seen in the Figure, in our link-budget we consider the effects of the full RF chain, from digital signal modulation to demodulation, including power amplifier and LNB considerations.

The rest of this section presents the equations used to compute the link-budget for a single beam. Further details about other aspects of the model can be found in [18].

We first compute the link C/N_0 as

$$\frac{C}{N_0} = P_{T_x} - \text{OBO} + G_{T_x} + G_{R_x} - L - 10\log_{10}(k\,T_{sys}) \quad [\text{dB}] \tag{1}$$

$$L = \text{FSPL} + L_{atm} + L_{RF_{T_x}} + L_{RF_{R_x}} \quad [\text{dB}] \tag{2}$$

where P_{Tx} is the transmitted power (dB), OBO is the power-amplifier output back-off, G_{T_x} and G_{R_x} are the transmitting and receiving antenna gains, respectively (dB), T_{sys} is the system temperature (K), and L is the sum of the losses considered, (dB). In particular, we consider free-space path losses (FSPL), atmospheric losses (L_{atm}), and losses in the transmitting and receiving RF chains ($L_{RF_{T_x}}$ and $L_{RF_{R_x}}$, respectively).

The system temperature is computed using Friis formula for noise temperature, as shown in Eq. 3:

$$\begin{aligned} T_{sys} = \; & T_{ant} \cdot 10^{-(L_{RF}/10)} + \\ & T_{atm} \cdot 10^{-(L_{atm}+L_{RF})/10} + \\ & T_w \cdot (1 - 10^{-(L_{RF}/10)}) \quad [\text{K}] \end{aligned} \tag{3}$$

where T_{ant} is the antenna temperature (K), T_{atm} is the atmospheric temperature (K), and T_w is the waveguide temperature (K). L_{atm} are the total atmospheric losses (dB), and L_{RF} are the RF losses in reception (dB).

Next, the link $E_b/(N+I)$ is computed as

$$\frac{C}{N_0 + I} = \left(\frac{1}{\text{CABI}} + \frac{1}{\text{CASI}} + \frac{1}{\text{CXPI}} + \frac{1}{\text{C3IM}} + \frac{1}{C/N_0} \right)^{-1} \tag{4}$$

$$\frac{E_b}{N+I} = \frac{C}{N_0 + I} \cdot \frac{BW}{R_b} \tag{5}$$

where R_b is the link data rate (see below) (bps) , and BW is the bandwidth allocated to that beam (Hz). Notice how our link budget equation considers four different types of interference (CABI, CASI, CXPI, and C3IM), which will be further described in the next section. In Eqs. 4 - 5, all terms are in linear scale.

Finally, the beam data rate is computed as

$$R_b = \frac{\text{BW}}{1+\alpha_r} \cdot \Gamma\left(\frac{E_b}{N+I}\right) \quad [\text{bps}], \tag{6}$$

where α_r is the roll-off factor, and Γ is the spectral efficiency of the modulation and coding scheme (MODCOD) (bps/Hz), which depends on the $E_b/(N+I)$ as described below.

In this study, we assume that adaptive coding and modulation (ACM) strategies are used, and therefore the MODCOD used on each link is the one that provides the maximum spectral efficiency and satisfies condition

$$\left.\frac{E_b}{N}\right|_{\text{th}} \geq \frac{E_b}{N+I} + \gamma \quad [\text{dB}], \tag{7}$$

where $\left.\frac{E_b}{N}\right|_{\text{th}}$ is the MODCOD threshold $E_b/(N+I)$ (dB), $\frac{E_b}{N+I}$ is the actual link energy per bit to noise plus interference ratio (dB) computed as indicated in Eq. 5, and γ is the desired link margin (dB) (In this paper we consider it to be zero). Note that in order to carry out the link-budget computations, one needs to assume *a-priori* that a given MODCOD scheme is used, compute Eqs. 1 - 6, and then verify whether condition in Eq. 7 is satisfied.

In this paper it is assumed that the satellites use the MODCOD schemes defined in the standard DVB-S2X [19], which corresponds to the second generation standard developed by the Digital Video Broadcast Project. This standard is the most popular for broadcasting, interactive services, and broadband services for space-based communications, and it defines the channel coding, framing structure, and modulation schemes to be employed. As part of the standard, a set of more than 60 MODCODs are provided, with modulation orders ranging from BPSK to 256-APSK, and coding rates ranging from 1/4 to 9/10.

Finally, to estimate the output back-off (OBO) for each of the MODCODs, we generate a synthetic sequence of 100,000 symbols and assume the OBO equals the peak-to-average power ratio of such a sequence (computed as the ratio between the 99.9th percentile power and the average power). Notice that this is an over-estimation of the required OBO, as in a real scenario, one could optimize the OBO value by simulating the channel and the RF chains in transmission and reception, as well as further reduce it by using pre-distortion techniques to push the amplifier closer to saturation.

Interference Models

Interference in multibeam systems is of vital importance, as due to the large differences in power among beams, it frequently becomes the limiting factor in the link budget of individual beams. In particular, we consider four different types of interference:

Carrier to adjacent beam interference (CABI): Occurs when multiple beams with overlapping bandwidths in the same satellite point to close locations while sharing the same polarization as the beam under study. This type of interference is computed as follows:

1. Determine the adjacent beams that have overlapping bandwidth with the beam under study. This includes beams with the same color and beams with different color and equal polarization that might have overlapping bandwidth as a consequence of the bandwidth allocation process. Add these beams to a list called `closest` (denoted as set $\mathcal{C}$).
2. For each beam:
   (a) Calculate, at 20 points of the beam's footprint contour, the sum of the interfering power from the beams in `closest`. To determine the received power from the `closest` beams we assumed a similar antenna radiation pattern to the one described in reference [20]:

$$G(\theta) = G_{max}\left(\frac{J_1(u)}{2u} + 36\frac{J_3(u)}{u^3}\right)^2 \tag{8}$$

where $u = 2.07123\frac{sin\theta}{sin\theta_{3dB}}$, θ is the angle between the beam center and the point of interest with respect to the satellite, θ_{3dB} is the one-sided half-power beamwidth, G_{max} is the maximum antenna gain, and J_1 and J_3 are Bessel functions of the first kind of order 1 and 3, respectively.
   (b) Calculate the CABI (in dB) as

$$\text{CABI} = 10\log_{10}\left(P_{\text{beam}}(p)\right) - 10\log_{10}\left(\sum_{b\in\mathcal{C}} P_b(p)\right), \tag{9}$$

where $P_{beam}(p)$ and $P_b(p)$ (dB) are the power of the beam under study and beam b, respectively, at point p, which corresponds to the point with the largest $\sum_{b\in\mathcal{C}} P_b(p)$ (i.e., we consider the worst-case interference).
(c) Re-compute the link budget using the newly calculated CABI.
3. If any beams' MODCOD has changed (and the current set of MODCODs for all beams is different from any previous set of MODCODs), go to step 2.

Carrier to adjacent satellites interference (CASI): Occurs when other satellites using the same frequency have beam footprints overlapping or close to the beam under study.

Carrier to cross polarization interference (CXPI): Occurs when a fraction of the same-frequency orthogonal-polarization signal interferes with the signal of the beam under study. We assume a fixed value of 30 dB for the CXPI, as suggested in [21].

Carrier to third order inter-modulation products interference (C3IM): Occurs due to the presence of multiple carriers with comparable frequencies and the non-linearities of the components of the RF chain. The C3IM is assumed to be 27 dB following the analysis in [22].

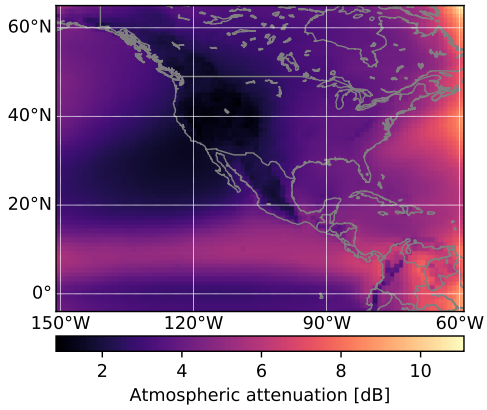

Figure 3: **Atmospheric attenuation exceeded during 5% of the time for the target region of the Viasat-1 scenario (see Section 5).**

Atmospheric Attenuation Model

Since each beam points to different regions of the Earth, atmospheric attenuation impacts each beam differently. We estimate the atmospheric attenuation effects using the ITU recommendations, which consider four different sources of atmospheric attenuation:

- **Rain attenuation:** The most important fading mechanism at communications satellites bands. Its magnitude is computed according to the guidelines provided in ITU-R P.618 [23].
- **Cloud attenuation:** Attenuation due to water or ice particles present in clouds, which absorb and scatter the signal. We compute the magnitude of this type of attenuation according to recommendation ITU-R P.840 [24].
- **Gaseous attenuation:** Caused by interactions of the electromagnetic waves with gas molecules. This attenuation is higher in the resonance frequencies of the molecules (e.g., 60 GHz band for oxygen molecules). Its value is computed following recommendation ITU-R P.676 [25].
- **Ionospheric scintillation attenuation:** Caused by radiation in the ionosphere, which results in rapid modification of the radio waves along with attenuation of the signal. It is computed according to recommendation ITU-R P.618 [23].

In all of the atmospheric attenuation computations, an availability percentage of 95% is employed. This parameter represents the fraction of time in which the atmospheric attenuation is lower than the given value. In other words, an availability of 95% implies that the atmospheric attenuation value computed using our model is surpassed only during 5% of the time. In this paper we use ITU-Rpy [26], a Python implementation of the ITU Recommendations, to compute the total atmospheric attenuation of Earth-to-space slant paths. Figure 3 shows the total atmospheric attenuation values exceeded during 5% of the time over America, using our implementation of the ITU models.

3. Problem Statement

We consider a satellite with N fixed-pointing beams, whose power and bandwidth can be dynamically allocated to satisfy the long-term estimated demand of each beam. The objective is to assign an average power and bandwidth to each of the N beams, such that the unmet system capacity (USC) is minimized, while satisfying a set of constraints imposed by the satellite.

Our figure of merit, the USC, represents the fraction of the demand that is *not* satisfied by the satellite, and is computed as indicated in Eq. 10 (note that there are no extra gains for offering a data rate that exceeds the demand). This metric is more suitable than its complement – the met system capacity (MSC) – because of its economic significance: communications satellite companies have to pay penalty fees when they fail to meet their customer service-level agreements (SLAs), and thus their interest in minimizing the USC. Moreover, this metric was used in this paper's baseline reference, [12], where it was chosen based on the comparison of several metrics carried out in [27].

$$USC = \sum_{b=1}^{N} max[D_b - R_b, 0] \tag{10}$$

Conceptually, the relationship between the MSC and the USC is shown in Fig. 4. As it can be seen, the sum of the MSC and the USC equals the demand, and if the demand is lower than the data rate, the USC is 0 (the MSC equals the demand).

In terms of constraints, we assume that the satellite has a total bandwidth B_{tot}, a total available power P_{tot}, and that the maximum transmit power per beam is P_b^{max}. As mentioned before, our objective is to minimize the USC (Eq. 10) by allocating power and bandwidth to beams in a satellite subject to the constraints. This can be formulated as the following mathematical program:

$$\underset{P_b,B_b}{\text{minimize}} \quad \text{USC}(P_b, B_b) \tag{11}$$

$$\text{subject to} \quad B_b \leq B_{tot} \qquad \forall b \in \mathcal{B} \tag{12}$$

$$P_b \leq P_b^{max} \qquad \forall b \in \mathcal{B} \tag{13}$$

$$\sum_{b=1}^{N} P_b \leq P_{tot} \tag{14}$$

$$B_a + B_b \leq B_{tot} \qquad \forall (a,b)_{adj,p} \tag{15}$$

where P_b and B_b are, respectively, the transmit power and bandwidth of beam b. $\mathcal{B}$ is the set of beams in the satellite, and N is the total number of beams. Equation 12 imposes the constraint that the bandwidth in any beam cannot exceed the satellite's total bandwidth. Equation 13 is needed to capture the saturation value of power amplifiers, while Eq. 14 ensures that beams do not use more power than what is available. Equation 15 is required to ensure that adjacent beams do not interfere, and is explained in more detail in Section 4.

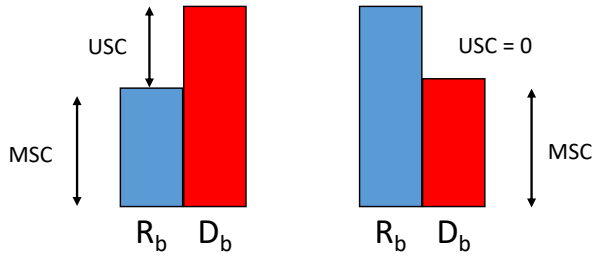

Figure 4: **Conceptual depiction of the MSC and USC metrics**

4. ALGORITHM

Proposed Solution: Genetic Algorithm

As demonstrated by Aravanis [12], the resource allocation (RA) problem stated in Section 3 (Eqs. 11-15) can be reduced to a special case of the sum rate maximization problem, which is NP-hard. Furthermore, since the sum rate maximization problem can be reduced to the maximum independent set problem (which is hard to approximate[2]), it is also true that the RA problem is hard to approximate [12]. Therefore, given that techniques which look for the optimal solution are computationally expensive, we turn to metaheuristic optimization methods.

Since the genetic algorithm used in [12] yielded better results than other techniques considered (such as simulated annealing, particle swarm optimization, or differential evolution methods), our solution adopts a similar approach; but in addition to allocating power to satellite beams, we also consider bandwidth allocation. The novel method developed in this paper is based on a genetic algorithm, a metaheuristic artificial intelligence technique inspired by biological evolution [28]. Throughout the algorithm, a set of N_{ind} "individuals" (i.e., allocations of power and bandwidth to every beam in the satellite) are generated and evolved through random processes similar to those found in nature, namely:

- **Mutation**: Attributes of the individual ind are randomly assigned new values, giving the algorithm the possibility to derive diverse solutions. Every individual has a probability p_{mut} of being altered by this operator. If applied, for each beam b, this operator assigns with probability p^i_{mut} a random value to P_b (chosen uniformly from 0 to P_b^{max}), and a random value of B_b (chosen uniformly from B_b^{min} to B_b^{max}).
- **Crossover**: The features of two individuals (referred to as the parents) are stochastically combined to generate a pair of new individuals (referred to as the *offspring*). This operator is applied with probability p_{xvr} to two consecutive elements (ind_1 and ind_2) in a shuffled list of individuals. Since both power and bandwidth are real numbers, we use blend crossover BLX-α [29], which creates two new individuals ind'_1 and ind'_2 by combining attributes x_1 from ind_1 and x_2 from ind_2, applying the following criterion:

$$\begin{aligned} x'_1 &= (1-\gamma)x_1 + \gamma x_2 \\ x'_2 &= \gamma x_1 + (1-\gamma)x_2 \end{aligned} \tag{16}$$

where γ is a random value chosen uniformly from $[-\alpha, 1+\alpha]$ (α is the parameter of BLX-α that determines the exploration/exploitation trade-off), and x'_1 and x'_2 are the attributes of ind'_1 and ind'_2, respectively, namely P_b and B_b. The resulting values for x'_1 and x'_2 are saturated so their value is in $[0, P_b^{max}]$ and $[B_b^{min}, B_b^{max}]$ respectively, when allocating power and bandwidth.
- **Selection of the fittest**: In every generation, before applying the mutation and crossover operators, the best individuals from the population are selected to become parents for the next generation. We use tournament-selection, which is carried out by picking the highest performing individual out of $tournsize$ randomly chosen individuals. This procedure is repeated N_{ind} times.

In our problem, each individual is represented as a vector containing N tuples, with each tuple consisting of a power and bandwidth allocation for a beam in the satellite. The fitness function is the USC (Eq. 11), which is to be minimized.

Algorithm 1 Genetic algorithm to allocate power and bandwidth

```
1:  function EVALUATE_SOLUTION(ind)
2:      ind ← constraint_handling(ind)
3:      sat ← Satellite(ind)
4:      sat.run_link_budget()
5:      return USC(sat)
6:
7:  pop ← list of N_ind individuals generated randomly
8:  for ind in pop do
9:      ind.USC ← evaluate_solution(ind)
10: gen ← 1
11: while gen ≤ N_gen do
12:     offspring ← selection_tournament(pop)
13:     offspring ← crossover_and_mutation(offspring)
14:     for ind in pop if ind.changed do
15:         ind.USC ← evaluate_solution(ind)
16:     pop ← offspring
17:
18:     stop ← convergence_criterion()
19:     if stop then
20:         break
21:     gen ← gen + 1
22: return pop
```

Algorithm 1 presents an overview of our algorithm. Initially, a population of individuals is created by assigning random values of power and bandwidth (within a certain range) to each of the beams, and then each individual is evaluated. Next, the following process is executed iteratively: for each generation, a subset of individuals from the population is selected, the crossover and mutation operators are applied, and then the new individuals are evaluated. The process continues until:

- Generation N_{gen} is reached. A maximum number of generations sets an upper limit for the algorithm's execution time, necessary so as to obtain solutions in a timely manner, or

[2]That is, approximation algorithms generate poor solutions.

• The convergence criterion is met, which consists of comparing the minimum USC of the current iteration against the minimum USC obtained in each of the last 30 iterations and stopping the procedure if the USC improvement is lower than a threshold value (*thresh*):

$$\left(\frac{USC_i - USC_{i-k}}{USC_i}\right) \cdot 100 \leq thres \quad \forall k = 1, ..., 30 \quad (17)$$

This convergence criterion has the advantage of setting an unbiased procedure to determine when to stop under different scenarios. It is customary to set a minimum number of generations N_{min} to guarantee that the algorithm performs a minimum exploration within the search space.

We implemented our genetic algorithm in Python, using the Distributed Evolutionary Algorithms in Python (DEAP) framework [30], together with the Python Standard Library multiprocessing package to speed up execution time, by parallelizing evaluations of the individuals' fitness functions in each generation. Because the algorithm assigns random values of power and bandwidth (within a certain range) to the beams when creating the initial population and when applying the mutation operation, invalid solutions might be generated occasionally (violating the constraints in Eq.12-15). Several techniques have been proposed to handle constraints in genetic algorithms, including rejection, reparation, and penalization of invalid individuals [31]. Our approach is to repair the incorrect solutions, by using different techniques to address the power constraint violations (as described in Eqs. 13 and 14), as well as to avoid bandwidth overlap. These techniques are described in the following lines of this section.

Power Constraints Handling

For the beam power, the constraints are shown in Eqs. 13 and 14. Equation 13 is guaranteed to be always satisfied since the initial generation, mutation, and crossover functions limit the values that the beam powers can take to within the [0, P_b^{max}] interval. On the other hand, if the sum of the beam powers P_{sum} exceeds P_{tot} (thereby violating Eq. 14), the beam powers are scaled down by multiplying them by a constant, $k = P_{tot}/P_{sum}$. By performing this multiplication, the powers are proportionally reduced so that the new P_{sum} is exactly equal to P_{tot}.

Bandwidth Constraints Handling

As for bandwidth, the constraint is that any pair of adjacent beams should not have overlapping frequencies, as shown in Eq. 15. That is:

$$B_a + B_b \leq B_{tot} \quad \forall (a, b)_{adj,p}$$

where B_a and B_b are the bandwidths allocated to beams a and b, B_{tot} is the total satellite bandwidth, and the subscript adj, p indicates that (a, b) are adjacent and equally-polarized beams. This constraint is enforced by applying the following procedure to every pair of adjacent beams with the same polarization, (a, b):

1. First, the starting beam is chosen between beam number 1 and number 37, with probability 0.5 assigned to each. When 1 is chosen as the initial beam, $b = a + 1$ (pairs are checked in increasing order, whereas when 37 is chosen, $b = a - 1$ (pairs are checked in decreasing order).
2. For each pair of beams (a, b), if $B_a + B_b > B_{tot}$, the algorithm assigns to $B_a = B_{tot} - B_b$ (that is, B_a is reduced). This procedure ensures that, when all pairs are handled, there are no violations of Eq. 18.

Applying this technique guarantees that the frequencies of equally-polarized adjacent beams will never overlap, but the genetic algorithm might leave bandwidth unused. Figure 5 depicts an example of this phenomenon for beams 1, 2 and 3 (see Fig. 6). The unused bandwidth between a triplet of beams can be calculated with Eq. 18:

$$B_{unused} = B_{tot} - B_c - max(B_l, B_r) \quad (18)$$

where B_{unused} is the unused bandwidth, B_{tot} is the total satellite bandwidth, and B_l, B_c, and B_r are the bandwidths of a triplet of adjacent beams (left, center, right).

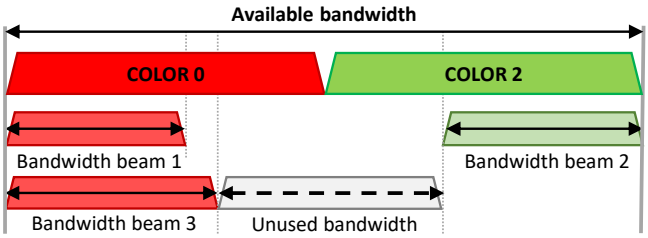

Figure 5: **Example of a case in which the bandwidth is not completely used in beams 1, 2 and 3.**

To maximize performance, the algorithm iterates over all the beams in decreasing order of demand and increases their bandwidth by adding B_{unused}, which is always higher than or equal to 0. After this procedure, it is assumed that there is neither interference due to overlapping frequencies nor unused bandwidth. Finally, the bandwidths are saturated so their value are in $[B_b^{min}, B_b^{max}]$.

5. Scenario Description

In this section, we provide the parameters used for the two case studies analyzed in this paper: a notional GEO satellite located at (0°, 25.8°E) with 37 spot beams (similar to the scenario analyzed in [12]), and a realistic case based on Viasat-1, a 72-spot-beam high-throughput satellite (HTS) covering North America.

37-beam GEO Satellite

Table 1 provides a summary of the parameters required for Eqs. 1-6. Atmospheric attenuation was not considered in this scenario to better reproduce the results in [12].

Figure 6 displays the footprint created by the satellite's beams. A four-color frequency reuse scheme (two bandwidth bands + dual polarization) is assumed. In the figure, beams assigned colors red and green use left-hand circular polarization (LHCP), while beams assigned colors yellow and blue use right-hand circular polarization (RHCP). In terms of bandwidth assignment, beams with different polarizations are independent, whereas adjacent beams that share the same polarization can trade bandwidths. Figure 7 shows an example: a red beam (e.g., beam 24) can increase its bandwidth if the green beams that are adjacent (beams 23 and 25) have their bandwidths reduced (as otherwise strong interference would occur, since adjacent beams use overlapping frequency intervals).

Viasat-1 Satellite

Viasat-1 is a 72-Ka-band spot-beam satellite located at orbital slot 115.1°W. The satellite, jointly owned by Viasat, Inc. and

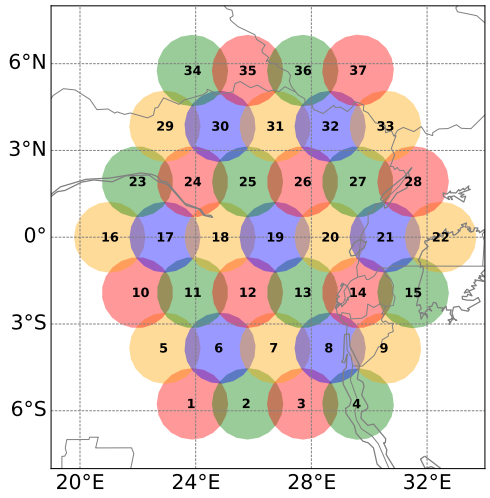

Figure 6: **Plot of the system of study: a satellite with 37 beams using a four-color frequency reuse pattern.**

Figure 7: **Colors and bandwidth diagram. Adjacent beams that have the same polarization can trade bandwidth.**

Table 1: **Link-budget and problem parameters for the 37-beam satellite case study.**

Parameter	Symbol	Value	Unit
Satellite altitude	h	35,786	km
Number of beams	n_{beams}	37	-
Payload power	P_{tot}	2350	W
Maximum power per beam	P_b^{max}	100	W
Central frequency	f	20	GHz
Total bandwidth	B_{tot}	375($\times$2 pol)	MHz
Tx antenna gain	G_{T_x}	52.2	dB
Tx antenna diameter	D_{T_x}	2.4	m
Output back-off	OBO	5	dB
Roll-off factor	α_r	0	-
Satellite EIRP	EIRP	63	dbW
Free-space path losses	FSPL	212	dB
Rx antenna gain	G_{R_x}	41.5	dB
Rx antenna diameter	D_{R_x}	0.7	m
System temperature	T_{sys}	211	K
LNB's noise figure	F	2.34	-
LNB's voltage standing wave ratio	VSWR	1.2	-
Carrier to adjacent satellite interference	CASI	28	dB
Carrier to cross polarization interference	CXPI	30	dB
Carrier to 3rd order intermodulation interference	C3IM	27	dB

Telesat, was launched in 2011 and is considered the first high-throughput satellite system in history, designed with a maximum throughput of 100 Gbps (under clear sky conditions). The payload allows for some flexibility in power allocation to the beams, but the bandwidth assigned to each beam is fixed. In this paper, we analyze the impact on performance of a flexible bandwidth allocation (as planned for next-generation satellites Viasat-2 and Viasat-3).

Figure 8 shows the beam footprint for the 61 continental US beams. Viasat-1 also uses a four-color frequency reuse scheme (two bandwidth bands + dual polarization); as in the 37-beam system, beams assigned colors red and green use left-hand circular polarization (LHCP), and beams assigned colors yellow and blue use right-hand circular polarization (RHCP).

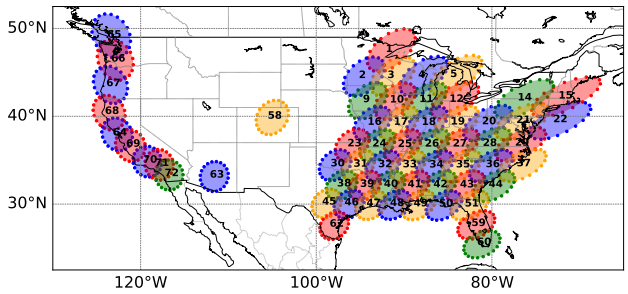

Figure 8: **Viasat-1 beam footprint. Only the 61 CONUS beams are displayed (beams over Alaska and Hawaii are not displayed).**

The parameters required for Eqs. 1-6 are summarized in Table 2. These are based on the link-budgets presented in the FCC public application filings for Viasat-1[3].

Table 2: **Link-budget and problem parameters for the Viasat-1 case study. Values *not* shown are identical to those shown in Table 1.**

Parameter	Symbol	Value	Unit
Satellite altitude	h	35,786	km
Number of beams	n_{beams}	63	-
Payload power	P_{tot}	10439	W
Maximum power per beam	P_b^{max}	300	W
Total bandwidth	B_{tot}	1,000($\times$2 pol)	MHz
Tx antenna gain	G_{T_x}	52.2	dB
Tx antenna diameter	D_{T_x}	2.6	m
Satellite EIRP	EIRP	60.7	dbW
Carrier to adjacent satellite interference	CASI	20.8	dB

Algorithm Parameters— Table 3 shows the values of the parameters for the algorithm described in Section 4. The same set of parameters was used for the 37-beam and Viasat-1 case studies.

[3] An example link budget for Viasat-1 is available at http://licensing.fcc.gov/myibfs/download.do?attachment_key=950366

Table 3: **Genetic algorithm parameters**

Parameter	Symbol	Value
Selection operator		Tournament
Crossover operator		BLX-α
Mutation operator		Uniform
Max. number generations	N_{gen}	750
Min. number of generations	N_{min}	75
Threshold	thresh	0.05%
Population size	N_{ind}	400
Tournament size	tournsize	5
Blend α	α_{xvr}	0.2
Crossover prob.	p_{xvr}	0.95
Mutation prob.	p_{mut}	0.05
Mutation ind. prob.	p^i_{mut}	0.15

6. RESULTS

37-beam GEO Satellite

Altogether, four different resource allocation strategies and two demand scenarios were considered, and for each case we ran 30 executions.

The first demand scenario reproduces the demand in [12], whereas the demand for the second scenario was synthetically generated to increase the variance in the beams' demand while keeping the total sum of the demand constant.

The four resource allocation strategies considered were:

- **Power allocation**: This is similar to the algorithm implemented in [12]. All beams are assigned a fixed bandwidth equal to 187.5 MHz (half of the total satellite bandwidth), but power in each beam is individually allocated.
- **Joint power and bandwidth allocation**: Both power and bandwidth are individually assigned, with the range of valid bandwidths for each beam limited to:
  - 30% to 70% of the total satellite bandwidth (B_{tot})
  - 20% to 80% of the total satellite bandwidth (B_{tot})
  - 0% to 100% of the total satellite bandwidth (B_{tot})

Results for the First Scenario: Moderate Demand Variation— For this case study, the same demand scenario as in [12] was used. The total data rate requested by the users under the 37 beams is 24.16 Gbps, whereas the standard deviation of the demands between beams is 177 Mbps.

The results are shown in Table 4. Under this demand scenario, the 30%-70% *joint power and bandwidth allocation* strategy yielded the best results on average, while the best run was one of the executions of the 20%-80% case. The average improvement in the USC when using *power allocation and uniform bandwidth*, compared to the case where power and bandwidth are both fixed, was 33.2%, while it was reported to be 54.3% in [12]. The smaller improvement obtained is likely due to the more careful modeling of the link-budget and interference in this paper. The average improvement of *jointly allocating power and bandwidth* compared to *allocating power alone* – shown in the third column – was around 33% for all cases, which indicates that even small variations of bandwidth can result in important improvements in terms of total system throughput. Moreover, the sum of beams' bandwidths was similar for both the *power allocation* and

Table 4: **Results for the moderate demand variation scenario. ΔUSC is the improvement in USC compared to the "Power allocation, uniform bandwidth" strategy. $\sum B_b$ represents the sum of the bandwidths of the individual beams. CNI is the carrier to noise plus interference ratio. P stands for total power, and # gen for the number of generations. The best average ΔUSC and the ΔUSC for the best execution are colored in green.**

Execution	USC [Gbps]	ΔUSC [%]	CNI [dB]	$\sum B_b$ [GHz]	P [W]	# gen
Uniform P and BW allocation	1.9	-	13.3	6.94	2349	-
Power allocation, uniform bandwidth						
Best run	1.21	-	13.0	6.94	2350	253
Worst run	1.36	-	13.2	6.94	2349	237
Average	1.27	-	13.1	6.94	2329	231.0
Std. deviation	0.035	-	0.1	0.0	28.7	10.96
Power and bandwidth allocation (0% - 100%)						
Best run	0.8	38.5	13.0	6.93	2233	226
Worst run	1.1	15.0	13.0	6.98	2209	225
Average	0.89	**31.4**	13.0	6.95	2194	230.7
Std. deviation	0.062	4.79	0.1	0.014	57.9	18.23
Power and bandwidth allocation (20% - 80%)						
Best run	0.74	42.8	13.1	6.94	2255	226
Worst run	1.26	3.3	13.0	6.97	2245	230
Average	0.86	**34.1**	13.0	6.95	2250	232.2
Std. deviation	0.118	9.09	0.0	0.014	35.5	19.44
Power and bandwidth allocation (30% - 70%)						
Best run	0.75	42.2	13.0	6.96	2215	239
Worst run	1.09	15.9	12.9	6.98	2189	225
Average	0.84	**35.2**	13.0	6.95	2253	228.5
Std. deviation	0.065	5.05	0.1	0.012	39.8	8.57

the *joint power and bandwidth allocation* strategies, which demonstrates that the reason allocating bandwidths yields better results is not that more bandwidth is actually used (as explained later), but that more bandwidth is assigned to those beams that have higher demand. As for the CNIs, note that they were very similar for all cases, including the *uniform power and bandwidth allocation*. Nevertheless, the *joint power and bandwidth allocation* cases yielded an improvement in the USC because resources were assigned more efficiently. Also note that, in addition to decreasing the USC (increasing system throughput), using a *joint power and bandwidth allocation* strategy resulted in lower total power consumption. This is because data rates on beams with high demands are delivered by assigning those beams a greater bandwidth, which is preferable to increasing their power since the latter will result in higher interference to neighboring beams.

The results shown next correspond to the best execution of the *joint power and bandwidth allocation* case (using the 20% - 80% range for the bandwidth allocation). Figure 10 depicts the algorithm's convergence by showing the maximum, average, and minimum values for the USC among the population. The algorithm stopped after 226 generations.

Figure 9 shows the data rate obtained with the *joint power and bandwidth allocation* algorithm, the data rate obtained with a *uniform power and bandwidth* allocation, and the

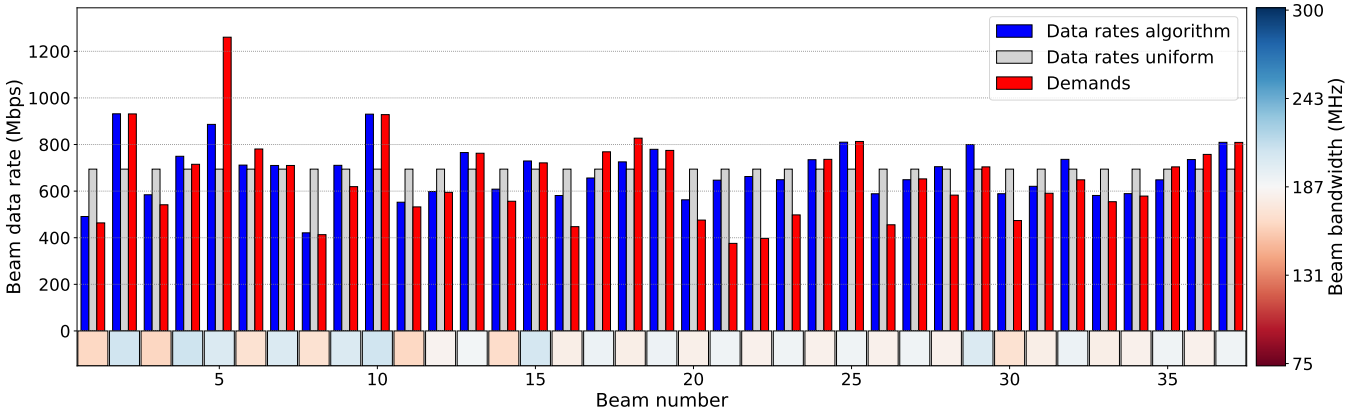

Figure 9: **Data rates for the best execution of the moderate demand variation scenario.**

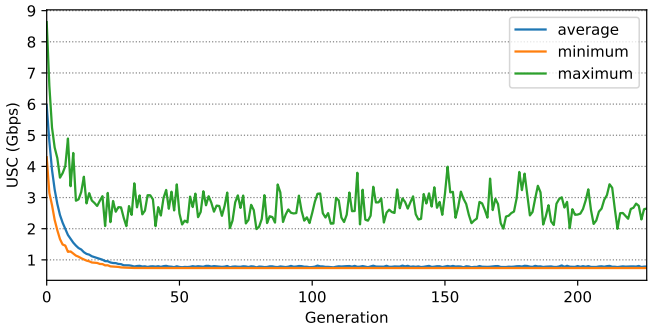

Figure 10: **Convergence for the best execution of the moderate demand variation scenario.**

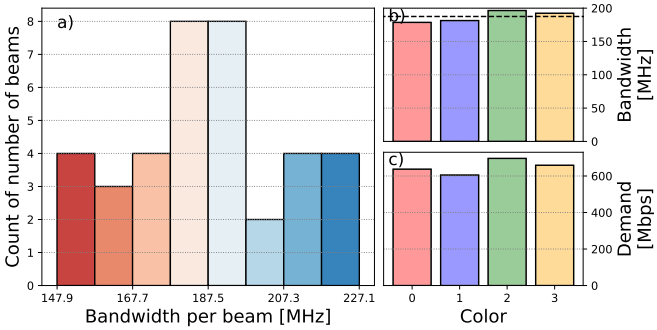

Figure 11: **a) Histogram of beam bandwidths, b) average beam bandwidth for each color, and c) total demand for each color for the best execution of the moderate demand variation scenario.**

demand per beam in blue, gray, and red, respectively. A black dot would be drawn above the data rate bar if a beam was assigned a power higher than 90% of P_b^{max}, which did not happen for any beam in this case. Notice how the data rate bars (blue) closely follow the demand bars (red). The bandwidth allocation values are shown with colored squares under the data rate bars. Normally, beams that present local demand maxima receive a higher-than-average bandwidth. Additionally, it can be observed that bandwidth is indeed traded between adjacent beams. For example, beams 1 to 4 present a pattern where the first beam has a lower-than-average bandwidth (thus colored in red), the second has a higher-than-average bandwidth (thus colored in blue), and so on.

Figure 11 presents a histogram of the bandwidths assigned to beams. Nineteen of them have less than 187.5 MHz (half the total satellite bandwidth), and 18 have more than this value. Note that the bar chart is close to symmetrical (since bandwidth is traded between beams). Fig. 11 also shows how the average beam bandwidth for each color roughly follows the total demand.

It can be observed in Table 4 that a small amount of bandwidth is sometimes "won" when using the *joint power and bandwidth allocation* strategy. When bandwidth is uniformly allocated, the total system bandwidth is $0.1875 \cdot 37 = 6.94$ GHz, whereas in the *joint power and bandwidth allocation* runs, the total bandwidth assigned to all 37 beams can be as high as 6.98 GHz (i.e., 40 MHz of bandwidth is "won"). Even though unintuitive at first glance, Fig. 12 shows an example that demonstrates how this could happen. The sum of the

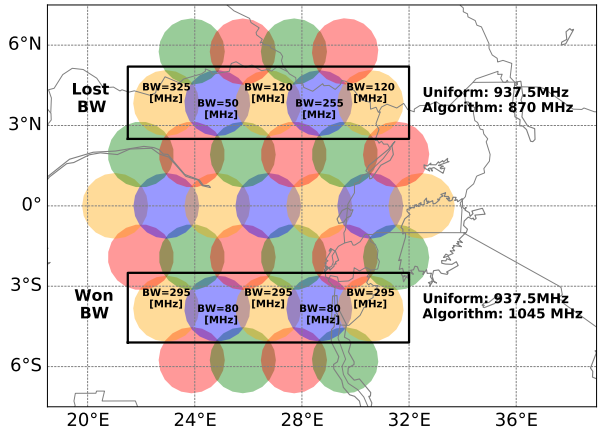

Figure 12: **Examples of scenarios where bandwidth is "won"and "lost".**

bandwidths of beams 5-9, the beams in the second-to-lowest row, is 1045 MHz instead of $187.5 \cdot 5 = 937.5$ MHz; that is, 107.5 MHz of bandwidth have been "won."

Additionally, as seen at the top of Fig. 12, our algorithm might also "lose" some bandwidth: the blue beam with $B_b = 50$ MHz is limited in bandwidth by the beam to its left ($325+50 = 375$ MHz), but has a "gap" of $375-(50+120) = 205$ MHz with the beam to its right, which in turn is limited

by its other adjacent beam. In this example, no beam could use more bandwidth than the allocated, but nevertheless the total bandwidth was 870 MHz while for a uniform bandwidth allocation it would have been $187.5 \cdot 5 = 937.5$ MHz. Interestingly, for the moderate demand variation scenario, this occurred only in the best *joint power and bandwidth allocation* 0% - 100% run, where approximately 10 MHz of bandwidth were "lost."

Results for the Second Scenario: High Demand Variation— This demand scenario was generated so that the total demand was equal – thus its average ($\bar{D}$) was also equal – to the previous case, but there was a higher variance between beams' demand. The procedure that generated the new demand profile is the following:

For each beam b with demand D_b:
1. With 50% probability, skip this beam. Beam b is also skipped if D_b has already been modified.
2. If $D_b \leq \bar{D}$, find a random beam b' such that $D_{b'} > \bar{D}$ and $D_{b'}$ has not been modified yet (if there is still one). If $D_b \geq \bar{D}$, do the opposite.
3. Between beams b and b', decrease the demand of the beam with lower demand and increase the demand of the beam with higher demand by a random value in the interval $[37.5\%, 62.5\%] \cdot D$, where $D = \min(D_b, D_{b'})$.
4. Mark D_b and $D_{b'}$ as modified.

The total data rate requested by the users under the 37 beams is, again, 24.16 Gbps, but the standard deviation of the demands between beams is 431 Mbps instead of 177 Mbps. Results for this scenario are shown in Table 5.

In this case, the *joint power and bandwidth allocation* strategy that produced the best average and overall results was the 0% - 100% case. Therefore, higher flexibility in the bandwidth assignments yields better results, which we believe is due to the higher variation in demand. Forcing the bandwidths to be bounded does not allow the algorithm the flexibility to assign higher values of bandwidth to the beams that present a higher demand, which results in poorer performance, as can be seen in the 20%-80% and 30%-70% results. The average improvement of the *power allocation*, with respect to the fixed power and bandwidth, was 16.8%, while the average improvement of *joint power and bandwidth allocation* compared to just *power allocation* was, for the 0-100 % case, 34.5%. Again, the total sum of bandwidths per beam and the average CNI values were similar for all cases, and the average total power was reduced when allocating power and bandwidth compared to a power-only allocation. Note that the average number of generations (230 - 250) is higher and presents a larger standard deviation than in the previous demand scenario, where the average number of generations was approximately 230 for all cases.

The results shown next correspond to the best execution for the high demand variation scenario, an execution of the *joint power and bandwidth allocation* 0% - 100% case.

Figures 13 depicts the algorithm's convergence, achieved after 226 generations.

Figure 14 shows the data rates obtained together with the demands. It can be observed that beams 13 and 29 were allocated more than 90% P_b^{max} and thus there is a black dot above their blue bars. In this case, the blue bars reach higher data rates due to the higher flexibility in bandwidth allocation. In fact, in the best case for the *moderate demand variation scenario*, the maximum data rate was approximately 950 Mbps, while in the *high demand variation scenario* the tenth beam provided almost 1,300 Mbps. Due to its very high demand, this beam received most of the available bandwidth while its only adjacent beam (number 11) had virtually no bandwidth assigned.

The histogram of bandwidths assigned to beams is shown in Fig. 15. Nineteen beams have less than 187.5 MHz (uniform bandwidth allocation) and 18 of them have more than 187.5 MHz. The histogram, as in the previous scenario, is close to symmetrical. In Fig. 15 b) and c) it can be seen that,

Table 5: Results for the high demand variation scenario. ΔUSC is the improvement in USC compared to the "Power allocation, uniform bandwidth" strategy. $\sum B_b$ represents the sum of the bandwidths of the individual beams. P stands for total power, and # gen for the number of generations. The best average ΔUSC and the ΔUSC for the best execution are colored in green.

Execution	USC [Gbps]	ΔUSC [%]	CNI [dB]	$\sum B_b$ [GHz]	P [W]	# gen
Uniform P and BW allocation	6.85	-	13.3	6.94	2349	-
Power allocation, uniform bandwidth						
Best run	5.65	-	12.7	6.94	2180	246
Worst run	5.77	-	12.8	6.94	2265	225
Average	5.7	-	12.7	6.94	2184	228.1
Std. deviation	0.034	-	0.1	0.0	44.3	7.13
Power and bandwidth allocation (0% - 100%)						
Best run	3.37	40.8	12.8	6.97	2095	226
Worst run	4.59	19.5	12.7	6.92	2231	225
Average	3.73	**34.5**	12.8	6.95	2126	237.0
Std. deviation	0.262	4.58	0.1	0.024	62.4	24.72
Power and bandwidth allocation (20% - 80%)						
Best run	3.72	34.7	12.7	6.94	2160	231
Worst run	4.37	23.3	12.8	6.92	2193	247
Average	3.98	**30.2**	12.7	6.95	2143	247.9
Std. deviation	0.17	2.99	0.1	0.018	48.2	33.22
Power and bandwidth allocation (30% - 70%)						
Best run	4.24	25.7	12.7	6.94	2193	225
Worst run	5.05	11.5	12.6	6.98	2119	227
Average	4.52	**20.6**	12.7	6.96	2146	243.6
Std. deviation	0.202	3.53	0.1	0.018	50.7	26.56

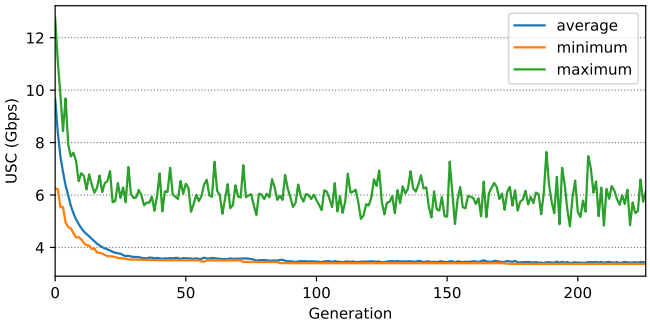

Figure 13: Convergence for the best execution of the high demand variation scenario.

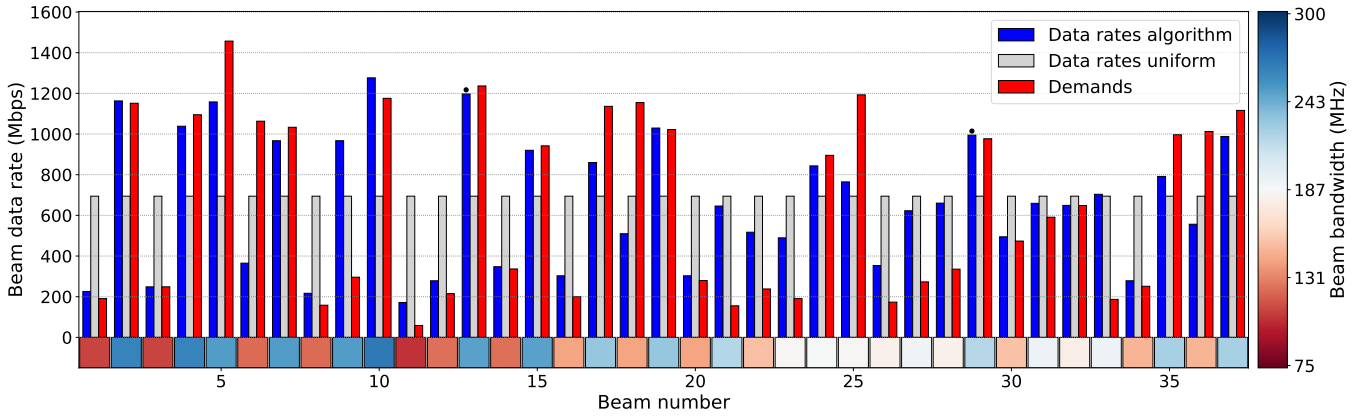

Figure 14: **Data rates for the best execution of the high demand variation scenario.**

even though blue beams present a slightly higher demand than yellow beams, yellow beams are allocated notably more bandwidth. A possible explanation is that they are located at both ends of every row in which they appear (e.g. see beams 5 and 9), and bandwidth can be "won" as shown in Fig. 12.

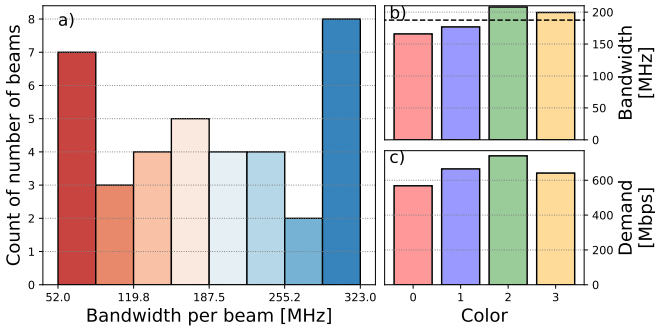

Figure 15: **a) Histogram of beam bandwidths, b) average beam bandwidth for each color, and c) total demand for each color for the best execution of the high demand variation scenario.**

Viasat-1 Satellite

As in the 37-beam case study, four different resource allocation strategies and two demand scenarios were considered in the Viasat-1 case study. For each case, we ran 20 executions.

The first demand scenario was chosen so that the demand on each beam was proportional to the population covered (assuming a total demand of 100 Gbps), while the demand for the second scenario was synthetically generated to increase the variance in the beams' demands, using a similar procedure as the one described for the 37-beam case study.

Results for the First Scenario: Demand proportional to population—In this scenario, the total data rate requested by the users under the 63 beams is 100.6 Gbps, whereas the standard deviation of the demands between beams is 0.8 Gbps.

The results are shown in Table 6. For this demand scenario, an average improvement of 11.2% was obtained when using the 0% - 100% *joint power and bandwidth allocation* strategy. In comparison to the 37-beam case study, the sum of beams' bandwidths was higher for the *joint power and bandwidth allocation* than for the *power allocation* strategy, and the total power consumption was also slightly higher for the *joint power and bandwidth allocation*. Thus, we believe that these two factors are driving the improvement in USC. In terms of average SNR, *joint power and bandwidth* strategies tend to yield values lower than the *power allocation* and *uniform power and bandwidth* strategies. This is an interesting result. Even though lower SNR values were obtained (in fact, the more flexibility in bandwidth allocation the lower the average SNR values), higher throughputs were achieved. This happens as having larger bandwidths allows for the use of lower-spectral-efficiency but higher-power-efficient MODCODs.

The results shown next correspond to the best execution of the *joint power and bandwidth allocation* case (using the 0%

Table 6: **Results for the moderate demand variation scenario in Viasat-1. The best average ΔUSC and the ΔUSC for the best execution are colored in green.**

Execution	USC [Gbps]	ΔUSC [%]	CNI [dB]	$\sum B_b$ [GHz]	P [W]	# gen
Uniform P and BW allocation	37.4	-	9.7	31.5	9134	-
Power allocation, uniform bandwidth						
Best run	28.0	-	8.9	31.5	7531	225
Worst run	28.6	-	9.8	31.5	9134	225
Average	28.2	-	9.4	31.5	8529	235.0
Std. deviation	0.14	-	0.5	0.0	707.7	15.0
Power and bandwidth allocation (0% - 100%)						
Best run	23.3	17.2	8.8	33.6	9134	390
Worst run	26.4	6.5	8.2	36.0	9134	265
Average	25.0	**11.2**	8.9	34.5	9133	257.5
Std. deviation	0.63	2.2	0.3	0.67	0.5	40.1
Power and bandwidth allocation (20% - 80%)						
Best run	24.6	12.8	9.2	31.7	9133	364
Worst run	27.2	3.6	9.2	31.4	9133	227
Average	25.9	**8.3**	9.2	32.6	9133	247.1
Std. deviation	0.63	2.25	0.2	0.59	0.5	31.6
Power and bandwidth allocation (30% - 70%)						
Best run	26.0	8.0	9.5	31.1	9134	236
Worst run	27.8	1.4	8.8	32.1	9134	323
Average	26.6	**5.6**	9.5	31.7	9133	242.6
Std. deviation	0.47	1.68	0.3	0.39	0.5	30.2

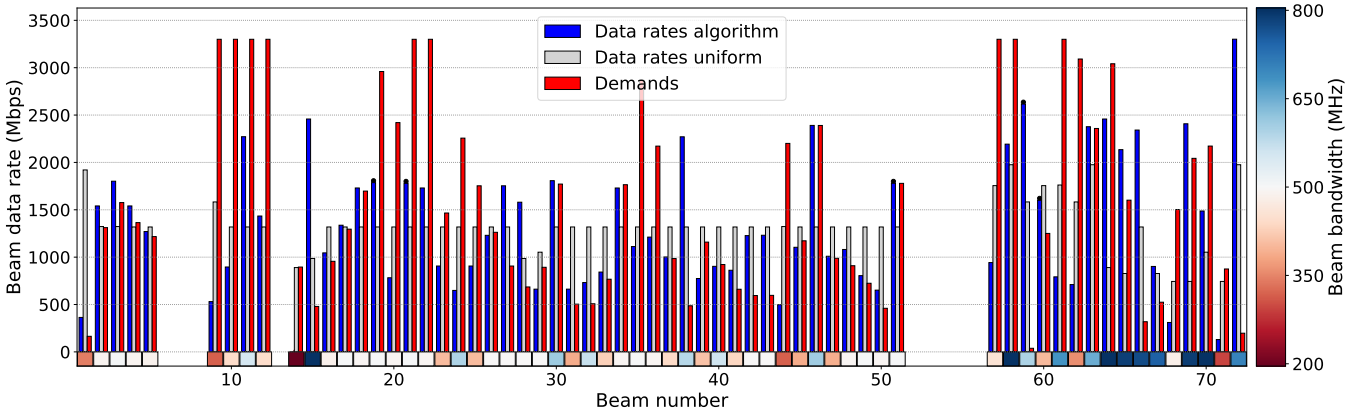

Figure 16: **Data rates for the best execution of the moderate demand variation scenario.**

- 100% range for the bandwidth allocation).

Figure 16 shows the data rate obtained with the *joint power and bandwidth allocation* algorithm, the data rate obtained with a *uniform power and bandwidth* allocation, and the demand per beam in blue, gray, and red, respectively. Since atmospheric attenuation was accounted for for this study, not all the uniform power and bandwidth data-rates are identical (gray bars). As in the previous cases, the data rate bars (blue) closely follow the demand bars (red) when using the joint power and bandwidth allocation. Beams 64-70 obtained the most gains in terms of bandwidth (as shown in Figure 16), because their footprint layouts allowed for the use of a two-color reuse scheme without incurring in adjacent beam interference penalties. Beams at very high latitudes (1-20) were the ones that benefited the least from flexible power and bandwidth allocation strategies, given that their highly deformed footprints are very susceptible to interference from neighboring beams.

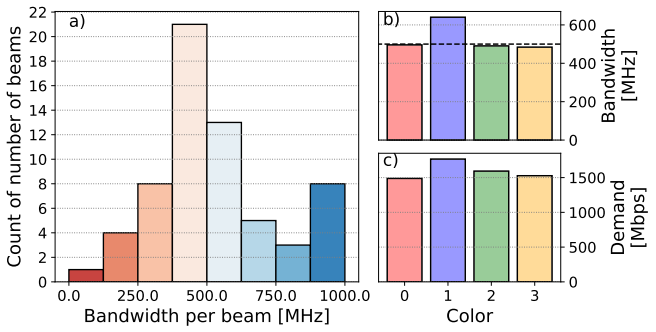

Figure 17: **a) Histogram of beam bandwidths, b) average beam bandwidth for each color, and c) total demand for each color for the best execution of the moderate demand variation scenario.**

Figure 17 presents a histogram of the bandwidths assigned to beams. 34 of them have less than 500 MHz (half the total satellite bandwidth), and 29 have a bandwidth higher than this value. In contrast to the 37-beam case study, the histogram is not symmetrical, since, as already mentioned, beams 64-70 can use a two-color reuse scheme and therefore have assigned bandwidths close to 1,000 MHz. Finally, note that even though the blue colored beams have the highest demands and average bandwidths, the allocations to the rest of the colors do not follow the average demand as closely as it did in the 37-beam case study, as shown in Figs. 17 b) and c).

Results for the Second Scenario: High Demand Variation— This demand scenario was generated so that the total demand was equal to the previous case, but there was a higher variance between beams' demand. The procedure used to generated the new demand profile was similar to the one previously described for the 37-beam case study. The total data rate requested by the users is, again, 100.6 Gbps, but the standard deviation of the demands between beams is 1.3 Gbps. Results for this scenario are shown in Table 7.

Table 7: **Results for the high demand variation scenario. The best average ΔUSC and the ΔUSC for the best execution are colored in green.**

Execution	USC [Gbps]	ΔUSC [%]	CNI [dB]	$\sum B_b$ [GHz]	P [W]	# gen
Uniform P and BW allocation	50.1	-	9.7	31.5	9134	-
Power allocation, uniform bandwidth						
Best run	39.6	-	8.3	31.5	7004	225
Worst run	40.0	-	7.9	31.5	6713	225
Average	39.8	-	8.0	31.5	6995	226.4
Std. deviation	0.12	-	0.5	0.0	602.1	6.3
Power and bandwidth allocation (0% - 100%)						
Best run	30.9	22.3	9.1	34.6	9134	225
Worst run	32.5	18.2	8.4	34.0	9128	228
Average	31.6	**20.7**	8.9	33.4	9096	243.3
Std. deviation	0.43	1.06	0.3	0.9	49.3	22.7
Power and bandwidth allocation (20% - 80%)						
Best run	32.6	18.1	9.1	32.4	8981	225
Worst run	33.9	14.9	10.0	30.1	8789	225
Average	33.2	**16.6**	9.4	31.3	9008	231.7
Std. deviation	0.34	0.84	0.4	0.79	124.8	11.9
Power and bandwidth allocation (30% - 70%)						
Best run	33.8	15.2	9.7	30.4	9036	225
Worst run	35.9	9.8	9.4	30.5	9059	225
Average	34.7	**12.8**	9.4	31.3	9047	232.6
Std. deviation	0.48	1.19	0.3	0.54	60.6	11.3

As in the 37-beam case study, the larger the variance in the demand between beams, the higher the improvement when allowing for larger flexibilities in the bandwidth allocations. The *joint power and bandwidth allocation* strategies that produced the best average results was the 0%-100% case. The average improvement of *joint power and bandwidth alloca-*

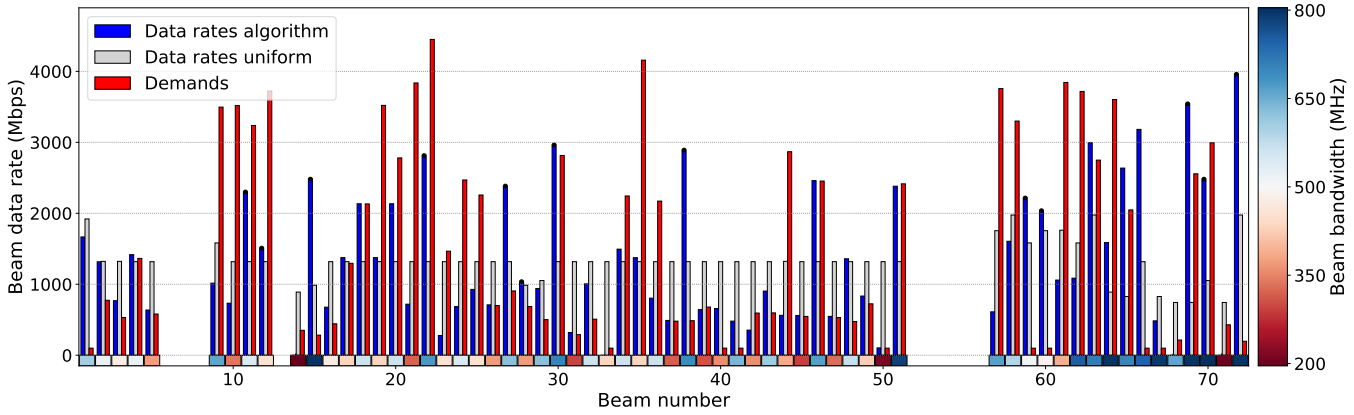

Figure 18: **Data rates for the best execution of the high demand variation scenario.**

tion compared to just *power allocation* was, for the 0-100% case, 20.7% (almost double the value of 11.2% obtained in the previous demand scenario), which shows that our method scales to realistic scenarios with tens of beams. Finally, allowing for bandwidth allocations resulted in an increase in the average SNR (from 8.0 dBs in the *power allocation allocation* to 8.9 dBs for the *joint power and bandwidth allocation* strategy). This is a surprising result, as the trend is opposite to the one exhibited in the previous demand scenario (see Table 6).

The results shown next correspond to the best execution for the high demand variation scenario, an execution of the *joint power and bandwidth allocation* 0% - 100% case.

Figure 18 shows the data rates obtained together with the demands. It can be observed that there is a much higher variation in bandwidth than in the previous demand scenario. Beams 1-20, which were previously allocated bandwidths close to 500 MHz (uniform bandwidth) showed a higher variance in bandwidth allocation, which in turn allows them to better follow the demand. As before, beams 64-72 got bandwidth allocations close to 100%, using a similar two-color frequency reuse pattern.

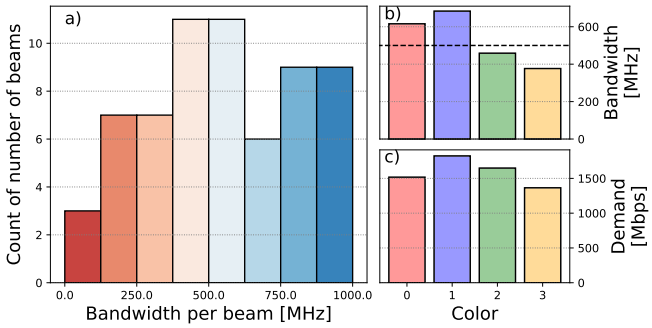

Figure 19: **a) Histogram of beam bandwidths, b) average beam bandwidth for each color, and c) total demand for each color for the best execution of the high demand variation scenario.**

The histogram of bandwidths assigned to beams is shown in Fig. 19. It can be observed that the range of bandwidths allocated is larger than in the previous case; approximately one fifth of the beams have bandwidths in the 0-300 MHz range, and one third in the 700-1,000 MHz range.

7. Conclusions

Summary

This paper explores the problem of joint power and bandwidth allocation in multibeam communications satellites subject to interference. The system model was presented in Section 2, and Section 3 formulated mathematically the problem this paper aimed to solve. Section 4 presented a genetic algorithm to jointly allocate power and bandwidth, subject to several constraints. Section 5 introduced two case studies, an academic 37-beam system used in previous research and a realistic scenario with the Viasat-1 satellite. Finally, the results obtained by performing simulations on both case-study problems were shown in Section 6. These results reveal that the USC can be reduced by an additional 40% by jointly allocating power and bandwidth, as opposed to using power-only allocation strategies. Moreover, we concluded that the higher the variations in demand among beams, the more beneficial it is to allow a greater flexibility in the range of bandwidth allocations allowed.

Main Findings

This paper has expanded the approach described in [12] to include bandwidth allocations in addition to power allocations. The main conclusions are:

- Apart from allocating power, the unmet system capacity (USC) can be further reduced by allocating bandwidths per beam.
- The approach taken in this paper to allocate both resources can reduce the USC further by 40% in the 37-beam case study and by 20% in the Viasat-1 case study, compared to a power-only allocation. This reduction can be achieved even using lower total bandwidths.
- The variability of the demand among beams has a strong impact on potential improvement: the higher the variability, the more important it is to allow our algorithm a greater flexibility in the range of bandwidth values.

Future Work

We envision the following possible extensions to this paper:

- With the advent of phased array antennas, the beam's shape and pointing direction will become additional variables to be determined by the DRM algorithm. Expanding our approach to be able to operate in such scenarios will be the main line of future work.
- Reinforcement learning and other machine learning tech-

niques have recently shown promising results in other resource allocation problems. Further exploration of their applicability and performance in communications satellites resource allocation problems is suggested.
- Even though the Viasat-1 case study showed that our algorithm successfully scales to scenarios with tens of beams, a study of how the algorithm further scales with the number of beams (and colors) could be beneficial, as it is foreseen that future communications satellites will have a much larger number of beams (hundreds and even thousands).

ACKNOWLEDGMENTS

The authors would like to thank the Centre de Formacio Interdisciplinaria Superior (CFIS) from the Universitat Politecnica de Catalunya (UPC) for partially funding this project.

REFERENCES

[1] L. J. Ippolito and L. J. Ippolito Jr, *Satellite communications systems engineering: atmospheric effects, satellite link design and system performance*. John Wiley & Sons, 2017.

[2] C. Balty, J.-D. Gayrard, and P. Agnieray, "Communication satellites to enter a new age of flexibility," *Acta Astronautica*, vol. 65, no. 1-2, pp. 75–81, 2009.

[3] SES S.A., "New frontiers annual report 2017," 2017.

[4] D. Whitefield and R. Gopal, "Capacity enhancement with dynamic resource management for next generation satellite systems," in *Military Communications Conference, 2005. MILCOM 2005. IEEE*. IEEE, 2005, pp. 761–767.

[5] P. Angeletti, D. Fernandez Prim, and R. Rinaldo, "Beam hopping in multi-beam broadband satellite systems: System performance and payload architecture analysis," in *24th AIAA International Communications Satellite Systems Conference*, 2006, p. 5376.

[6] J. Anzalchi, A. Couchman, P. Gabellini, G. Gallinaro, L. D'agristina, N. Alagha, and P. Angeletti, "Beam hopping in multi-beam broadband satellite systems: System simulation and performance comparison with non-hopped systems," in *Advanced satellite multimedia systems conference (ASMA) and the 11th signal processing for space communications workshop (SPSC), 2010 5th*. IEEE, 2010, pp. 248–255.

[7] A. Kyrgiazos, B. Evans, and P. Thompson, "Smart gateways designs with time switched feeders and beam hopping user links," in *Advanced Satellite Multimedia Systems Conference and the 14th Signal Processing for Space Communications Workshop (ASMS/SPSC), 2016 8th*. IEEE, 2016, pp. 1–6.

[8] S. Kandeepan, L. De Nardis, M.-G. Di Benedetto, A. Guidotti, and G. E. Corazza, "Cognitive satellite terrestrial radios," in *proc. IEEE Global Telecommunications Conference (GLOBECOM)*, 2010, pp. 1–6.

[9] S. K. Sharma, S. Maleki, S. Chatzinotas, J. Grotz, J. Krause, and B. Ottersten, "Joint carrier allocation and beamforming for cognitive SatComs in Ka-band (17.3–18.1 GHz)," in *Communications (ICC), 2015 IEEE International Conference on*. IEEE, 2015, pp. 873–878.

[10] E. Lagunas, S. K. Sharma, S. Maleki, S. Chatzinotas, and B. Ottersten, "Resource allocation for cognitive satellite communications with incumbent terrestrial networks," *IEEE Transactions on Cognitive Communications and Networking*, vol. 1, no. 3, pp. 305–317, 2015.

[11] L. N. Wang and B. Wang, "Distributed power control for cognitive satellite networks," in *Advanced Materials Research*, vol. 490. Trans Tech Publ, 2012, pp. 1156–1160.

[12] A. I. Aravanis, B. S. MR, P.-D. Arapoglou, G. Danoy, P. G. Cottis, and B. Ottersten, "Power allocation in multibeam satellite systems: A two-stage multi-objective optimization," *IEEE Transactions on Wireless Communications*, vol. 14, no. 6, pp. 3171–3182, 2015.

[13] J. Lei and M. A. Vazquez-Castro, "Joint power and carrier allocation for the multibeam satellite downlink with individual sinr constraints," in *Communications (ICC), 2010 IEEE International Conference on*. IEEE, 2010, pp. 1–5.

[14] Z. Ji, Y. Wang, W. Feng, and J. Lu, "Delay-aware power and bandwidth allocation for multiuser satellite downlinks," *IEEE Communications Letters*, vol. 18, no. 11, pp. 1951–1954, 2014.

[15] Y. He, Y. Jia, and X. Zhong, "A traffic-awareness dynamic resource allocation scheme based on multi-objective optimization in multi-beam mobile satellite communication systems," *International Journal of Distributed Sensor Networks*, vol. 13, no. 8, 2017.

[16] H. Wang, Z. Liu, Z. Cheng, Y. Miao, W. Feng, and N. Ge, "Maximization of link capacity by joint power and spectrum allocation for smart satellite transponder," in *Communications (APCC), 2017 23rd Asia-Pacific Conference on*. IEEE, 2017, pp. 1–6.

[17] H. Wang, A. Liu, and X. Pan, "Optimization of joint power and bandwidth allocation in multi-spot-beam satellite communication systems," *Mathematical Problems in engineering*, vol. 2014, 2014.

[18] A. París i Bordas, "Power and bandwidth allocation in multibeam satellite systems," B.S. thesis, Universitat Politècnica de Catalunya, 2018.

[19] Digital Video Broadcasting (DVB), "Implementation guidelines for the second generation system for broadcasting, interactive services, news gathering and other broadband satellite applications; Part 2 - S2 extensions (DVB-S2X)," 2015.

[20] M. A. Díaz, N. Courville, C. Mosquera, G. Liva, and G. E. Corazza, "Non-linear interference mitigation for broadband multimedia satellite systems," in *Satellite and Space Communications, 2007. IWSSC'07. International Workshop on*. IEEE, 2007, pp. 61–65.

[21] ETSI EN, "DVB Document A171-2 - Digital Video Broadcasting (DVB) Implementation guidelines for the second generation system for Broadcasting, Interactive Services, News Gathering and other broadband satellite applications;Part 2 - S2 Extensions (DVB-S2X)," Technical report, Tech. rep., ETSI, Tech. Rep., 2015.

[22] M. Aloisio, P. Angeletti, E. Casini, E. Colzi, S. D'Addio, and R. Oliva-Balague, "Accurate characterization of TWTA distortion in multicarrier operation by means of a correlation-based method," *IEEE Transactions on electron devices*, vol. 56, no. 5, pp. 951–958, 2009.

[23] International Telecommunication Union Radiocommunication Sector (ITU-R), "Recommendation ITU-R P.618-12: Propagation data and prediction methods re-

quired for the design of earth-space telecommunication systems," 2015.

[24] ——, "Recommendation ITU-R P.840-6: Attenuation due to clouds and fog," 2013.

[25] ——, "Recommendation ITU-R P.676-11: Attenuation by atmospheric gases," 2016.

[26] I. del Portillo, "ITU-Rpy: A python implementation of the ITU-R P. recommendations to compute atmospheric attenuation in slant and horizontal paths." https://github.com/iportillo/ITU-Rpy/, 2017.

[27] A. I. Aravanis, G. Danoy, P. Arapoglou, P. G. Cottis, and B. Ottersten, "Multi-objective optimization approach to power allocation in multibeam systems," in *30th AIAA International Communications Satellite System Conference (ICSSC)*, 2012, p. 15202.

[28] M. Mitchell, *An introduction to genetic algorithms*. MIT Press, 1998.

[29] L. J. Eshelman and J. D. Schaffer, "Real-coded genetic algorithms and interval-schemata," in *Foundations of genetic algorithms*. Elsevier, 1993, vol. 2, pp. 187–202.

[30] F.-A. Fortin, F.-M. De Rainville, M.-A. Gardner, M. Parizeau, and C. Gagné, "DEAP: Evolutionary algorithms made easy," *Journal of Machine Learning Research*, vol. 13, pp. 2171–2175, jul 2012.

[31] B. Craenen, A. Eiben, and E. Marchiori, "How to handle constraints with evolutionary algorithms," *Practical Handbook Of Genetic Algorithms: Applications*, pp. 341–361, 2001.

BIOGRAPHY

Aleix Paris *is a graduate student pursing his M.S. in the Department of Aeronautics and Astronautics at MIT. He received two degrees from Universitat Politecnica de Catalunya, Barcelona, in Aerospace Engineering and Computer Science (2018). His research interests include autonomous systems, space systems, and artificial intelligence.*

Inigo del Portillo *is a Ph.D. candidate in the department of Aeronautics and Astronautics at MIT. His research interests include system architectures for spacial and aerial concepts to extend global connectivity, space optical communications systems, and small satellites communications. Inigo received his degrees in Industrial Engineering, Electronics Engineering and Telecommunications Engineering in 2014 from Universitat Politecnica de Catalunya, Barcelona, and his M.Sc. in Aeronautics and Astronautics from MIT in 2016.*

Dr. Bruce Cameron *is a Lecturer in Engineering Systems at MIT and a consultant on platform strategies. At MIT, Dr. Cameron ran the MIT Commonality study, a 16 firm investigation of platforming returns. Dr. Cameron's current clients include Fortune 500 firms in high tech, aerospace, transportation, and consumer goods. Prior to MIT, Bruce worked as an engagement manager at a management consultancy and as a system engineer at MDA Space Systems, and has built hardware currently in orbit. Dr. Cameron received his undergraduate degree from the University of Toronto, and graduate degrees from MIT.*

Dr. Edward F. Crawley *received an Sc.D. in Aerospace Structures from MIT in 1981. His early research interests centered on structural dynamics, aeroelasticity, and the development of actively controlled and intelligent structures. Recently, Dr. Crawley's research has focused on the domain of the architecture and design of complex systems. From 1996 to 2003 he served as the Department Head of Aeronautics and Astronautics at MIT, leading the strategic realignment of the department. Dr. Crawley is a Fellow of the AIAA and the Royal Aeronautical Society (UK), and is a member of three national academies of engineering. He is the author of numerous journal publications in the AIAA Journal, the ASME Journal, the Journal of Composite Materials, and Acta Astronautica. He received the NASA Public Service Medal. Recently, Prof Crawley was one of the ten members of the presidential committee led by Norman Augustine to study the future of human spaceflight in the US.*